

COMPARISON OF UNCERTAINTY PARAMETERISATIONS FOR \mathcal{H}_∞ ROBUST CONTROL OF TURBOCHARGED DIESEL ENGINES

Merten Jung^{*,1} Keith Glover^{*} Urs Christen^{**}

** University of Cambridge, Trumpington Street,
Cambridge, CB2 1PZ, UK*

*** Ford Forschungszentrum Aachen, Süsterfeldstraße 200,
52072 Aachen, Germany*

Abstract: This paper investigates the effect of the uncertainty parameterisation type on the performance of \mathcal{H}_∞ robust controllers for diesel engine airpath control. A comparison between the experimental and simulated frequency responses indicates that the main uncertainty lies in the three parameters commonly perceived as being difficult to model in this application. Different approaches to parameterise the observed uncertainty are compared and evaluated. Based on an extended \mathcal{H}_∞ loopshaping procedure, two degrees of freedom controllers will be designed using μ synthesis tools; one for a general coprime factor uncertainty description, the others for application tailored uncertainty parameterisations. The controllers are compared based on μ analysis and experimental results.

Keywords: \mathcal{H}_∞ loopshaping, μ synthesis, uncertainty parameterisation

1. INTRODUCTION

The \mathcal{H}_∞ loopshaping procedure by McFarlane and Glover (McFarlane and Glover, 1992) has become increasingly popular in recent years. This methodology comprises two steps: Firstly, the scaling and weighting of the multivariable plant with pre- and postcompensators to shape the frequency response. Thus, engineers can use their experience and knowledge of the plant characteristics to obtain a trade-off between performance and robust stability. Secondly, the stability radius of the shaped plant is optimised with respect to coprime factor uncertainty. The reason for using this class of uncertainty is that it is very general and includes a wide class of other unstructured uncertainty types, e. g. additive and multiplicative uncertainty.

The question addressed in this paper is whether additional knowledge about the uncertainty can be used to improve the controller performance. This issue arose during the model validation for a turbocharged diesel engine (cf. Sections 2 and 3). Mismatches in the frequency responses of the model and experimental data could be ascribed to parametric uncertainties as described in Section 4. After designing a conventional two degrees of freedom \mathcal{H}_∞ loopshaping controller for coprime factor uncertainty in Section 5, the knowledge about the structure of the uncertainty will be used for several tailored uncertainty descriptions in Section 6. A state-space approach turns out to be least conservative and is then used to compare the controller performances based on a real μ analysis in Section 7. This analysis indicates the superior performance of the controller designed for the application tailored uncertainties compared

¹ corresponding author, Jung@tu-harburg.de

to the conventional one, which is confirmed by experimental results.

2. THE CONTROL PROBLEM

The plant to be controlled is a turbocharged passenger car diesel engine equipped with exhaust gas recirculation as depicted in Figure 1. The turbocharger increases the power density of the engine by forcing air into the cylinders, which allows injection of additional fuel without reaching the smoke limit. The turbine, which is driven by the energy in the exhaust gas, has a variable geometry (VGT) that allows the adaptation of the turbine efficiency based on the engine operating point.

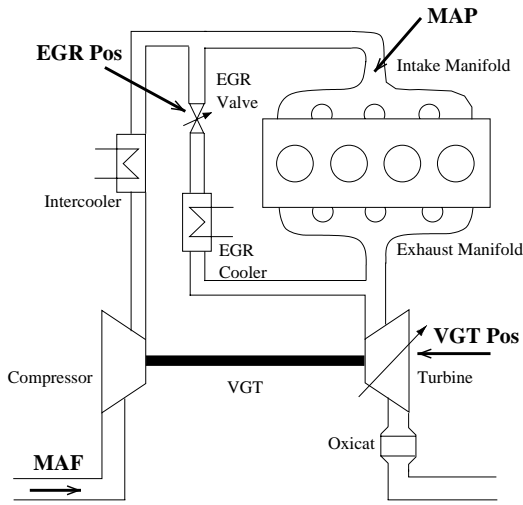


Fig. 1. Diesel engine setup.

The second feedback path from the exhaust to the intake manifold is due to exhaust gas recirculation (EGR), which is controlled by an EGR valve. The recirculated exhaust gas replaces oxygen in the inlet charge, thereby reducing the temperature profile of the combustion and hence the emissions of oxides of nitrogen. The interactions are relatively complex; a detailed description can be found in (Ladommatos *et al.*, 1996) and the references therein.

While the VGT actuator is typically used to control the intake manifold absolute pressure (MAP), the EGR valve controls the mass air flow (MAF) into the engine. Both the EGR and VGT paths are driven by the exhaust gas and hence constitute an inherently multivariable control problem.

3. DIESEL ENGINE MODEL

An eighth order nonlinear model of the airpath of the diesel engine in Figure 1 can be derived as follows:

- The **intake and exhaust manifolds** are modelled as open thermodynamic systems where the mass of gas can increase or decrease with time (so-called *filling and emptying model*). The governing equations for such systems are the *Conservation of Mass* and the *Conservation of Energy* leading to first order differential equations for the manifold pressures and accumulated masses.
- The mass flow from the intake manifold into the **cylinders** is described by the so-called *speed-density equation* which statically models the engine pumping.
- The **exhaust gas recirculation (EGR) system** is modelled statically by a standard orifice flow equation with the orifice effective area (A_{orif}) depending on the EGR valve position.
- The **variable geometry turbocharger (VGT)** is described by a differential equation for the turbocharger shaft speed based on a power balance between the turbine and compressor side. In order to calculate the compressor and turbine power, their efficiencies (η_c, η_t) and mass flows have to be known. They are provided by the supplier in form of static nonlinear maps based on pressure ratios, turbocharger speed and VGT actuator position. These maps are then parameterised for use in the model.
- The pneumatic **EGR and VGT actuators** are driven by underlying PI controllers. These position control loops are identified as first order lags with a bandwidth of 1 Hz and 0.5 Hz for the EGR and VGT actuator, respectively.

A complete derivation of the model with focus on the turbocharger parameterisation can be found in (Jung *et al.*, 2002).

4. UNCERTAINTY INVESTIGATION

In order to apply linear control design methodologies, the nonlinear model described in the previous section has to be linearised at a fixed operating point. Figure 2 shows the frequency response of the model linearised at 1500 rpm, 85 Nm (solid lines) along with the experimentally obtained frequency response at that operating point (crosses). For the latter, the system was excited with a sum of sinusoids applied to the EGR and VGT actuator separately while measuring the response in MAF and MAP. The frequency response is then obtained from the input and output FFTs. Note that due to the limited bandwidth of the actuator position control loops, the maximal frequency for the identification has been chosen as 1 Hz.

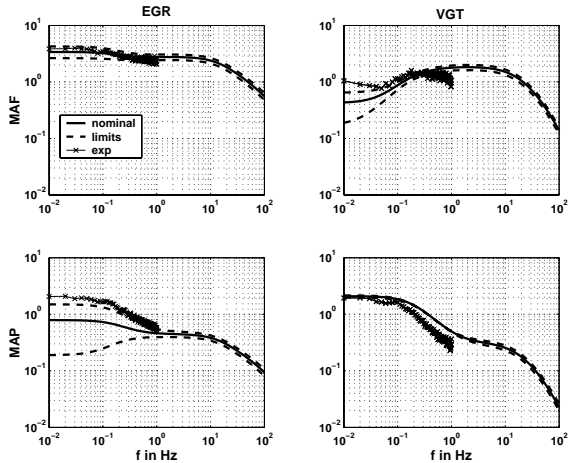


Fig. 2. Frequency response of the scaled plant at 1500 rpm, 85 Nm and with varied parameters (worst-case combination of $\pm 15\%$ changes in η_c , η_t , and A_{orif}).

Figure 2 shows quite good agreement between the simulation and experimental data in the main couplings, i.e. from EGR to MAF and VGT to MAP, especially in the low frequency range (this is not surprising since the model has been parameterised with steady-state data). However, there are significant deviations over a wide frequency range in the cross-couplings, i.e. from EGR to MAP and VGT to MAF.

In order to better understand the differences between the modelled and the identified frequency responses, the sensitivity of the model is investigated with respect to parameter changes. This is done by increasing and decreasing the parameter values in the nonlinear model by $\pm 15\%$. It turns out that most of the parameters only have a minor effect on the frequency response. However, three parameters (the turbine and compressor efficiencies as well as the effective area of the EGR valve) do have a significant effect. Moreover, this effect turns out to be exactly where the differences between the simulation and experiment have been observed, namely in the low frequency range of the cross-couplings. While the efficiencies mainly affect the EGR to MAP channel, the effective area of the EGR valve influences the VGT to MAF channel. Figure 2 also shows the boundaries that are obtained from the worst-case combination of the three parameter changes (dashed lines).

Note that the parameters identified to have the biggest effect are the ones that one would suspect to be most uncertain. The modelling in (Jung *et al.*, 2002) has shown that the turbocharger efficiencies are most difficult to parameterise, and the uncertainty in the effective area of the EGR valve stems from the fact that it has been identified from averaged experimental data and parameterised as a nonlinear function of the valve lift. Moreover, the orifice model for the EGR valve is

only a crude approximation of the true phenomena; all the unmodelled effects are lumped into the effective area. Both the efficiencies and the effective area cannot be measured directly.

5. \mathcal{H}_∞ LOOPSHAPING CONTROL

This section describes the \mathcal{H}_∞ loopshaping design methodology proposed in (McFarlane and Glover, 1992) with the example of the diesel engine airpath control problem at hand, for which a two degrees of freedom controller is required to achieve satisfactory performance.

5.1 Choice of Weights

The MAF and MAP loops have different speeds in response, hence the magnitude plots are shaped in this application rather than the singular values. The precompensator W_1 is chosen as PI weight for both channels to achieve zero steady-state error. The zeros of the PI weights are placed at the intended closed-loop bandwidths (which have been selected as approximately 0.4 Hz for the EGR loop and 0.2 Hz for the VGT loop) to stop the roll-off and hence to avoid additional phase lag at cross-over. Finally, constant gains in both channels are chosen such that the cross-over frequencies of the shaped plant coincide with the targeted closed-loop bandwidths of each channel. A postcompensator is not needed since the plant rolls off naturally.

Typically, it is desired to increase the bandwidth of the scaled plant. However, this is not possible here since the scaled plant contains the actuator position control loops (1.0 Hz bandwidth for the MAF channel and 0.5 Hz bandwidth for the MAP channel). Hence, the bandwidth of the closed-loop system has to be lower than that of the inner actuator loops. This is reflected in the targeted bandwidths of 0.4 Hz for the MAF channel and 0.2 Hz for the MAP channel. In order to make the system response faster, a two degrees of freedom approach will be taken.

5.2 Two Degrees of Freedom Design

A two degrees of freedom extension of the \mathcal{H}_∞ loopshaping methodology was proposed by Limebeer *et al.* (Limebeer *et al.*, 1993). It allows the design of a feedback controller to robustly stabilise the plant with respect to coprime factor uncertainty and of a dynamic prefilter to make the closed loop match a reference model in a single step. The design configuration is depicted in Figure 3, which is an extension of the standard framework. The transfer matrices (\tilde{M}, \tilde{N}) are assumed

to be a left coprime factorisation of the shaped plant, i. e. $P_s = \tilde{M}^{-1}\tilde{N}$. Note that ρ is a tuning factor that weighs the relative importance of the model matching against the robust stabilisation.

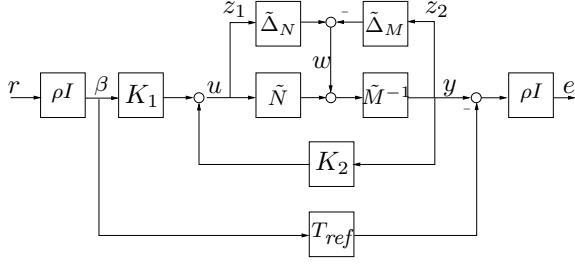


Fig. 3. Two degrees of freedom \mathcal{H}_∞ loopshaping configuration.

The reference model for the model matching of the closed loop is chosen as first order lag with the same bandwidths as the underlying actuator position control loops (1.0 and 0.5 Hz, respectively). The cross-couplings in the reference model are chosen to be zero to decouple the channels; the steady-state gain is unity as required by reference tracking.

5.3 Controller Synthesis

The robust performance problem at hand is tackled by the D-K iteration technique, cf. (Zhou *et al.*, 1996). The synthesised controller $K = [K_1, K_2]$ has ten states, the same as the generalised plant (six states from the engine model, which has been model reduced, two states from the precompensator, and two states from the reference model). Note that K_1 and K_2 share the same state space. For this and the subsequent μ synthesis designs, the scaling matrices D are chosen to be static to keep the controller order as low as possible (the scaling matrices are absorbed into the generalised plant during the synthesis leading to a higher controller order when increasing the order of their dynamic fit). Note that increasing the order of the scalings did not significantly improve the achieved μ values.

6. UNCERTAINTY PARAMETERISATIONS

As described in the previous section, the \mathcal{H}_∞ loopshaping methodology optimises the robustness of the system with respect to coprime factor uncertainty. The reason for using this class of uncertainty is that it is very general and includes a wide class of other unstructured uncertainty types, e. g. additive and multiplicative uncertainty. The question to be addressed in this section is how to incorporate an uncertainty description tailored to the application, i. e. taking advantage of the extra knowledge in Figure 2, which shows where

the main uncertainties occur in the model of the EGR-VGT system.

Ideally, the uncertainty would be parameterised directly based on the parameters in the nonlinear model that are known to be most uncertain, i. e. the effective area of the EGR valve and the efficiencies of the turbine and compressor. However, these parameters (especially the turbocharger efficiencies) are rather complicated polynomial functions of the inputs and states of the system. Hence, the linearised model is used subsequently to obtain an uncertainty description.

6.1 Additive Uncertainty

A straightforward approach to derive an uncertainty description is to parameterise the uncertainty based on the frequency responses and error bounds in Figure 2 directly. The weighted plant is therefore augmented with an additive uncertainty which replaces the coprime factor uncertainty in Figure 3. The plant plus uncertainty represent a class of models P_Δ obtained by adding weighted uncertainty to the nominal shaped model P_s :

$$P_\Delta(s) = P_s(s) + W_{\Delta_2}(s)\Delta_u(s)W_{\Delta_1}(s),$$

$$\|\Delta_u(s)\|_\infty < 1,$$

where W_{Δ_1} and W_{Δ_2} are stable transfer matrices that characterise the spatial and frequency structure of the uncertainty. Note that due to the additive nature, the same uncertainty description of the unshaped plant would be different, i. e. the loopshaping weights affect the uncertainty description, which is not true in the case of multiplicative uncertainty. However, in this application with the uncertainties mainly occurring in the cross-couplings, the additive uncertainty description is easier to obtain.

Figure 4 shows the frequency responses of the nominal shaped plant (solid lines) and of the shaped plant with varied parameters (dotted lines). Again, the uncertainty is largest in the low frequency range of the cross-couplings. In order to construct the uncertainty weights W_{Δ_1} and W_{Δ_2} , the uncertainty bounds are obtained for the system by plotting the error

$$\Delta_{err}(j\omega) = P_\Delta(j\omega) - P_s(j\omega),$$

where P_s corresponds to the nominal (shaped) frequency response (solid lines in Figure 4) and P_Δ to the frequency responses with worst-case parameter combinations (dotted lines, upper and lower limit) implying $\|\Delta_u(s)\|_\infty = 1$. This approach assumes that the frequency responses for smaller parameter variations are captured by $\|\Delta_u(s)\|_\infty < 1$, which seems reasonable. The additive error Δ_{err} then has to be bounded by fitted transfer functions, subsequently referred to as matrix

W_{fit} . A good fit can be obtained by second and third order transfer functions (increasing the resulting controller order by six). Using these fits, the uncertainty bounds on the shaped plant are plotted in Figure 4 (dashed lines). The good agreement gives confidence that they describe the uncertainty rather well.

For the control design, the fitted additive uncertainty has to be factorised into the form $W_{\Delta_2}\Delta_u W_{\Delta_1}$:

$$\begin{aligned} & \begin{pmatrix} \delta_1 W_{fit_{11}} & \delta_2 W_{fit_{12}} \\ \delta_3 W_{fit_{21}} & \delta_4 W_{fit_{22}} \end{pmatrix} \\ &= \begin{pmatrix} W_{fit_{11}} & W_{fit_{12}} & 0 & 0 \\ 0 & 0 & W_{fit_{21}} & W_{fit_{22}} \end{pmatrix} \times \\ & \quad \times \begin{pmatrix} \delta_1 & & & \\ & \delta_2 & & \\ & & \delta_3 & \\ & & & \delta_4 \end{pmatrix} \begin{pmatrix} 1 & 0 \\ 0 & 1 \\ 1 & 0 \\ 0 & 1 \end{pmatrix} \\ & := W_{\Delta_2}(s)\Delta_u(s)W_{\Delta_1}(s), \|\Delta_u(s)\|_\infty < 1, \delta_i \in \mathbb{C}. \end{aligned}$$

The four different scalars $\delta_1, \dots, \delta_4$ imply that each element in W_{fit} changes independently as Δ_u varies. Since the uncertainty that originally arose from three real parameters is now covered by four complex parameters implies that this parameterisation is rather conservative. Nevertheless, it will turn out to be useful for control design.

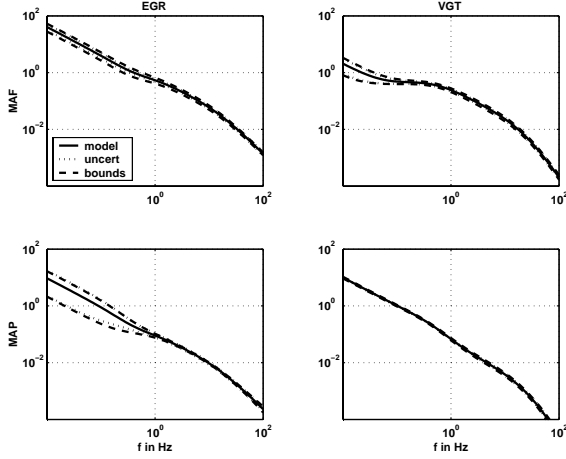


Fig. 4. Frequency response of the shaped plant with varied parameters and additive uncertainty bounds.

6.2 Parametric State-Space Uncertainty

For this approach, the nonlinear model is linearised for separate changes in each of the three parameters. Their effect on the nominal state-space model (A, B, C, D) is then expressed as follows

$$G_\delta(s) = \left(\begin{array}{c|c} A + \sum_{i=1}^3 \delta_i \hat{A}_i & B + \sum_{i=1}^3 \delta_i \hat{B}_i \\ \hline C + \sum_{i=1}^3 \delta_i \hat{C}_i & D + \sum_{i=1}^3 \delta_i \hat{D}_i \end{array} \right),$$

where $\delta_i \in [-1, 1]$ and the matrices $\hat{A}_i, \hat{B}_i, \hat{C}_i, \hat{D}_i$ reflect how the i 'th uncertainty, δ_i , affects the state-space model. This uncertainty description can then be reformulated to obtain an LFT representation as described e.g. in (Zhou *et al.*, 1996). In this case, the uncertainty block is obtained as

$$\Delta_u = \text{diag}\{\delta_1 I_4, \delta_2 I_2, \delta_3 I_1\},$$

where δ_1 corresponds to the effective EGR valve area, δ_2 and δ_3 to the compressor and turbine efficiency, respectively. Thus, the uncertainty is expressed by three real parameters rather than by four complex ones as in the case of the additive uncertainty description. However, it remains to confirm that a combination of the uncertainty parameters results in a valid uncertainty description. This is done by plotting the frequency response for simultaneously changed parameters. A comparison of Figure 5 to Figure 2 proves the validity of this approach.

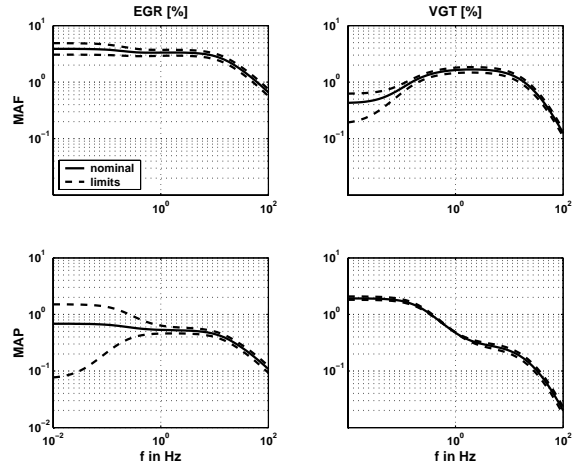


Fig. 5. Frequency response of the scaled plant at 1500 rpm and 85 Nm and the limits with worst-case parametric state-space uncertainty.

6.3 'Pulling Out the Deltas' Approach

An alternative solution is to use the fact that the turbocharger efficiencies mainly affect the turbocharger speed, which is a state of the model, and the effective area is a static nonlinear function of the EGR actuator position and can thus be regarded as a model input.

Then, using the linearised model, it is possible to extract the uncertainties of the turbocharger speed state and the effective area input; a process, which is sometimes referred to as *pulling out the*

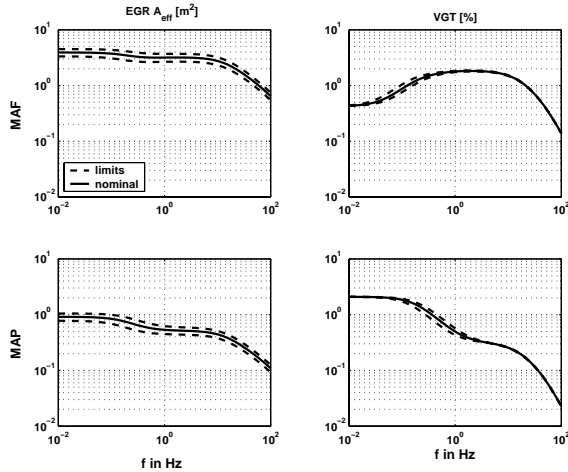


Fig. 6. Frequency response of the scaled plant at 1500 rpm and 85 Nm and the limits with worst-case 'pulled out deltas'.

deltas (Zhou *et al.*, 1996). From nonlinear simulations it can be derived how much the turbocharger speed varies with changes in the efficiencies. The same can be done for the effective area and the actuator position. Thus, a linearised model with parametric uncertainty is constructed.

However, comparing the frequency responses obtained for maximal deviation of the parameters in Figure 6 to the results for worst-case parameter changes in the nonlinear model in Figure 2, it turns out that the linear uncertainty description does not capture the effects in the nonlinear model, i. e. the nonlinear changes are too significant to be captured by this linear approach. Note that the EGR input in Figure 6 is the effective area of the valve, not the actuator position, hence the scaling had to be adjusted.

7. CONTROLLER COMPARISON

In order to assess the effect of the tailored uncertainty descriptions, robust two degrees of freedom controllers have been designed for the additive uncertainty (AUC) and the parametric state-space uncertainty (SSUC). Note that the latter results in a mixed μ synthesis which can be tackled by a (D,G)-K iteration that includes a G scaling to exploit the phase information given by the real parameters, cf. (Young, 2001). To allow for a fair comparison to the coprime factor uncertainty controller (CUC) from Section 5, the same weights and reference models have been used. This led to quite conservative designs so that the parameterised uncertainties were downscaled until the time domain performances were identical in nonlinear simulation.

7.1 Real μ Analysis

All three controllers (CUC, AUC, SSUC) are now analysed based on the parametric state-space uncertainty description from Section 6.2 containing only three real parameters and therefore being the least conservative. The setup for the analysis is shown in Figure 7. The robustness and performance are analysed via the transfer functions from w to z and r to e , respectively. Note that W_i is a constant scaling matrix to make the closed-loop transfer function from r to y match the reference model exactly at steady-state.

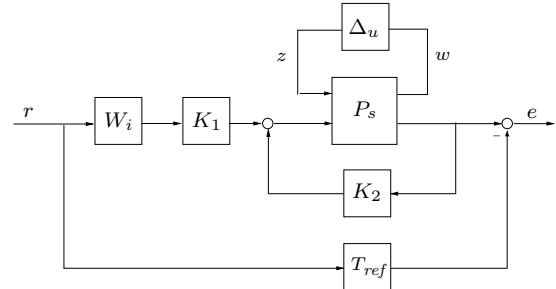


Fig. 7. Setup for μ analysis.

The results of the real μ analysis are shown in Figure 8. The μ plot (left) shows that the peak μ value is reduced by 46% from 1.16 for the CUC to 0.63 for the AUC and to 0.55 for the SSUC. The plot on the right side of Figure 8 shows the graphs for robust stability and nominal performance. It reveals that the large μ value for the CUC is due to the nominal performance, while the robust stability is almost exactly the same for both controllers. This indicates that for the tighter additive uncertainty description, the minimisation can focus on the performance.

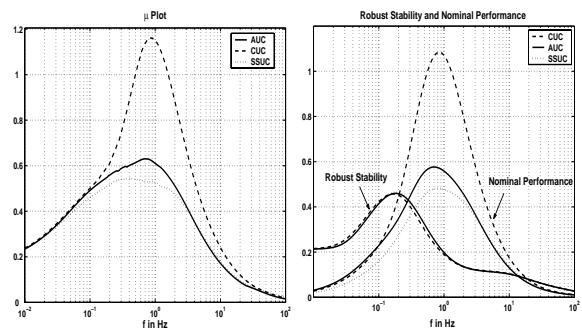


Fig. 8. Comparison of μ plots (left) and robust stability as well as nominal performance (right) of the state-space uncertainty (magenta) to the additive uncertainty (solid) and coprime uncertainty controller (dashed).

The main improvement in the μ plots for the SSUC is obtained by having one parameter less. The further restriction to those parameters being real rather than complex only results in very little further improvement. This is due to the fact that

the peak μ value occurs at around 1 Hz where the robust stability is already excellent and the peak is due to the nominal performance block.

7.2 Load Step Responses

In this section, the performance of the controllers are compared with respect to a load change of ± 35 Nm around the nominal operating point at fixed engine speed (1500 rpm). The reference values for MAP and MAF are stored in an ECU map based on speed and fuelling and hence change simultaneously. Figure 9 depicts the responses.

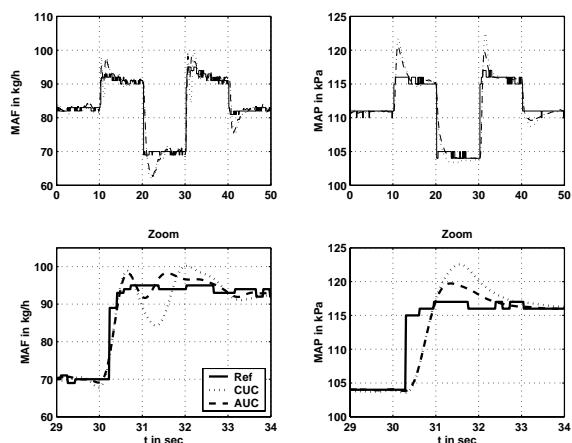


Fig. 9. Comparison of CUC and AUC controllers with respect to load changes (85 ± 35 Nm).

The different responses in Figure 9 confirm the observations from the μ analysis. The coprime uncertainty controller causes significant overshoot in the MAP channel and oscillatory behaviour in the MAF channel (dotted lines). The same response times but with less overshoot and oscillation is achieved with the additive uncertainty controller (dashed lines), which reduces the mean-square tracking error by 22%. This again confirms the suitability of this approach.

The performance of the SSUC is almost identical to the AUC and therefore not plotted. Further validation results confirm the findings of this section but have to be omitted due to lack of space.

8. CONCLUSIONS

This paper has derived and compared different uncertainty parameterisations for the coordinated control of the airpath of a turbocharged diesel engine. Based on these parameterisations, two degrees of freedom \mathcal{H}_∞ loopshaping controllers have been designed: one with respect to general coprime factor uncertainty (CUC), the others

with respect to application tailored additive uncertainty (AUC) and parametric state-space uncertainty (SSUC), respectively.

A real μ analysis based on the parametric state-space uncertainty description indicates the superior robust performance of the controllers designed for the tailored uncertainty descriptions. Experimental validation shows that these controllers achieve better decoupling and less overshoot for the same response time compared to the CUC. Hence, the knowledge about the structure of the uncertainty included in the uncertainty description is indeed useful. These physically motivated uncertainty parameterisations are more accurate than the general coprime factor approach and allow for a better control design.

ACKNOWLEDGEMENTS

The principal author acknowledges financial support in part by the European Commission through the program Training and Mobility of Researchers - Research Networks and through project System Identification (FMRX CT98 0206) and acknowledges contacts with the participants in the European Research Network System Identification (ERNSI). Additional financial and technical support from the Ford Motor Company is also gratefully acknowledged. Many thanks to Peter Young for providing (D,G)-K iteration software.

REFERENCES

- Jung, M., R. Ford, K. Glover, N. Collings, U. Christen and M. Watts (2002). Parameterization and transient validation of a variable geometry turbocharger for mean-value modeling at low and medium speed-load points. *Society of Automotive Engineers*.
- Ladommatos, N., S. Abdelhalim, H. Zhao and Z. Hu (1996). The dilution, chemical, and thermal effects of exhaust gas recirculation on diesel engine emissions — part 1: Effect of reducing inlet charge oxygen. *Society of Automotive Engineers*.
- Limebeer, D., E. Kasenally and J. Perkins (1993). On the design of robust two degree of freedom controllers. *Automatica* **29**, 157–168.
- McFarlane, D. and K. Glover (1992). A loop shaping design procedure using \mathcal{H}_∞ synthesis. *IEEE Transactions on Automatic Control* **37**, 759–769.
- Young, P. M. (2001). Structured singular value approach for systems with parametric uncertainty. *International Journal of Robust and Nonlinear Control* **11**, 653–680.
- Zhou, K., J. Doyle and K. Glover (1996). *Robust and Optimal Control*. Prentice-Hall, New Jersey.